Applied Clay Science 146 (2017) 388–396

Contents lists available at ScienceDirect

Applied Clay Science

journal homepage: www.elsevier.com/locate/clay

Research paper

Two synthesis approaches of Fe-containing intercalated montmorillonites: Differences as acid catalysts for the synthesis of 1,5-benzodeazepine from 1, 2-phenylenediamine and acetone

Beatriz González[a], Raquel Trujillano[a], Miguel A. Vicente[a,*], Antonio Gil[b], Valentina N. Panchenko[c,d], Ekaterina A. Petrova[d], Maria N. Timofeeva[c,d,*]

[a] Departamento de Química Inorgánica, Universidad de Salamanca, Salamanca, Spain
[b] Departamento de Química Aplicada, Universidad Pública de Navarra, 31006 Pamplona, Spain
[c] Boreskov Institute of Catalysis SB RAS, Prospekt Akad. Lavrentieva 5, 630090 Novosibirsk, Russian Federation
[d] Novosibirsk State Technical University, Prospekt K. Marksa 20, 630092 Novosibirsk, Russian Federation

ARTICLE INFO

Keywords:
Fe,Si-montmorillonite composites
Fe,Al-pillared montmorillonite
1,5-Benzodiazepine
1,2-Phenylenediamine
Cyclocondensation reaction

ABSTRACT

Two approaches were considered for the preparation of Fe-containing composites based on montmorillonite and comparison of their structural, physicochemical and catalytic properties. The first approach (Si,Fe_x-Mt materials) was based on the intercalation of Cheto montmorillonite (Mt) by 3-aminopropyltriethoxysilane (APTES) and $FeCl_3$ via the sol-gel polymerization technique. Fe/Si atomic ratios were 6:94, 18:82 and 30:70. Then Si,Fe_x-Mt materials were calcined in air at 400 or 500 °C for the APTES removal. The second approach ($Al_{13-x}Fe_x$-Mt materials, x = 1 and 2) was based on the pillaring method using Keggin type mixed $Al_{13-x}Fe_x$-polycation (x = 1, 2) and montmorillonite from Cheto, Arizona, USA (Mt) as starting material. The intercalated $Al_{13-x}Fe_x$-Mt materials were calcined at 400 or 500 °C. The physicochemical characterization pointed out the effectiveness of the incorporation of Fe and Si into the interlayer space of the clay mineral. The fixation of small amounts of Fe (1.9 wt%) increased the basal space from 9.57 to 13.89 Å, but the further fixation of Fe content slightly decreased the basal space. The specific surface area increased from 80 up to 171 m^2/g. The oligomeric state of Fe_2O_3 particles depended on its content; the larger Fe content, the larger particle size of Fe_2O_3. Catalytic properties of Si,Fe_x-Mt and $Al_{13-x}Fe_x$-Mt materials were studied in the cyclocondensation of 1,2-phenylenediamine with acetone to 1,5-benzodiazepine. The yield of 1,5-benzodiazepine was found to rise with increasing of the Fe content in Si,Fe_x-Mt. Catalytic performance of Si,Fe_x-Mt was lower in comparison with $Al_{13-x}Fe_x$-Mt, that is in agreement with the amount of Lewis acid sites.

1. Introduction

Nowadays the design of new porous materials attracts the attention of researchers working in the fields of adsorption and catalysis. Clay minerals are one of the most attractive materials for generation of such solids due to their unique structural, textural and physicochemical properties, i. e. the high microporosity and specific surface area (150–350 m^2/g), the possibility of variation of acid-base properties, etc. Several procedures have been performed in order to improve these properties; thus, the properties of clay minerals can be modulated selecting the modification method, and in each method, varying several parameters. In the case of smectites, the difficulty of controlling a permanent interlayer space is an important disadvantage, as their dehydration at ~250 °C gives rise to the collapse of the layers, which makes the interlayer space inaccessible, limiting their applicability (Bergaya and Lagaly, 2013).

The intercalation chemistry of smectites is a very attractive field for preparing catalysts or catalyst supports alternative to zeolites and zeotype materials. Intercalation can produce materials with improved thermal resistance and stability, development of microporosity, high surface area and increased numbers of Brønsted and Lewis acid sites (BAS and LAS). Species as various as polycations, metallic complexes, alkoxides, biomolecules or polymers, among others, have been used for modification of clay minerals, particularly in the case of smectites, in which the interaction should be by cation exchange, hydrogen or van der Waals bonds, or covalent bonds, with or without expansion of the interlayer space. A particular functionalization treatment is silanization, silanes with different substituents (as amine, mercapto or

* Corresponding authors at: Departamento de Química Inorgánica, Universidad de Salamanca, Salamanca, Spain.
E-mail addresses: mavicente@usal.es (M.A. Vicente), timofeeva@catalysis.ru (M.N. Timofeeva).

http://dx.doi.org/10.1016/j.clay.2017.06.028
Received 25 April 2017; Received in revised form 22 June 2017; Accepted 24 June 2017

chlorine) have been used for functionalization of clay minerals, silanization occurring by reaction of the alkoxy groups with the -OH present on the surface of the clays (Avila et al., 2010; Wayde et al., 2011; Moreira et al., 2017).

On contrast, the preparation of pillared interlayered clays (PILC) is based in the cation exchange of the original charge compensating cations of smectites by metallic polyoxocations, which are subsequently thermally transformed into stable metallic clusters grafted to the clay layers. The intercalation of large polyoxometalates and the subsequent calcination of the intercalated solids thus obtained give rise to stable structures with constant interlayer space up to high temperatures. The pillar formation permits to improve the textural properties by the creation of interlayer spaces and active acidic and metallic centres, and adequate porosity to be used in catalysis applications (Gil et al., 2010; Vicente et al., 2013).

Benzodiazepines and their derivatives are an important class among the nitrogen-containing heterocyclic compounds with biological activity, being widely used in medicine as antidepressants, analgesic and sedative compounds, among other uses (Schutz, 1982). Moreover, they can be used as intermediates for the synthesis of other biological compounds, such as oxadiazole derivatives (Xu et al., 1999; Nabih et al., 2004) and triazole (Essaber et al., 1998; Bennamane et al., 2008). One of the ways for the synthesis of 1,5-benzodiazepines is the reaction of condensation of 1,2-phenylenediamines with ketones in the presence of both Brønsted acids (Reddy and Sreekanth, 2003; Tajbakhsh et al., 2006; Kaur and Gagandeep, 2013) and Lewis acids (Yadav et al., 2005; Pasha and Jayashankara, 2006). Systems with metals adsorbed on the surface of solid supports can also be used as catalysts for this reaction. Thus, Chari and Syamasunder (2005) demonstrated that the reaction of 1,2-phenylenediamines with ketones to 1,5-benzodiazepine can be catalyzed by $FeCl_3$ supported over poly(4-vinylpyridine) polymer. Unfortunately, no data were reported on the effect of the Fe content and surface acidity on the reaction rate and yield of 1,5-benzodiazepine.

Fe-containing intercalated montmorillonites may also be used as catalysts for this reaction due to the existence of surface acid sites (Timofeeva and Mel'gunov, 2009; Timofeeva et al., 2010). Thus, two series of Fe-containing intercalated montmorillonites were prepared in the present work by two different synthetic ways. The first series of Fe-containing materials (Si,Fe-Mt) was synthesized by sol-gel polymerization technique using montmorillonite (Mt) from Cheto, Arizona, USA as starting material, 3-aminopropyltriethoxysilane (APTES) and $FeCl_3{\cdot}6H_2O$ as sources of Si and Fe, in aqueous medium. Such type of materials was prepared for the first time. The second series of Fe-containing materials (Al,Fe-Mt) was prepared by the pillaring method using Mt as starting material and Keggin type mixed $Al_{13-x}Fe_x$-polycation (x = 1, 2). Al,Fe-Mt and Si,Fe-Mt materials were calcined at 400 or 500 °C in air for the generation of layer-columnar structure. These systems should have different acid-base properties and, therefore, different catalytic behavior, reason by which their catalytic properties were compared in the cyclocondensation of 1,2-phenylenediamine (I) with acetone to 2,3-dihydro-2,2,4-trimethyl-1H-1,5-benzodiazepine (III) (Scheme 1). Special attention has been paid to the estimation of the catalytic potential of these materials.

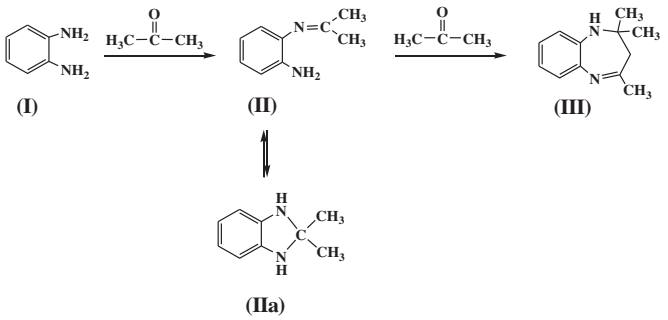

Scheme 1. The cyclocondensation of 1,2-phenylenediamine with acetone.

2. Experimental

2.1. Materials

Commercial methanol, acetone and 1,2-phenylenediamine (Acros Organics), 3-aminopropyltriethoxysilane (APTES), $FeCl_3{\cdot}6H_2O$ and $AlCl_3{\cdot}6H_2O$ (Sigma-Aldrich), all of maximum purity, were used as received, without any purification treatment.

The clay mineral used for the preparation of the pillared samples was the montmorillonite (Mt) from Cheto, Arizona, USA (The Clay Minerals Repository, where this sample is denoted as SAz-1). The raw clay mineral was purified before its use by dispersion-decantation, separating the ≤ 2 μm fraction (the clay was not submitted to other activation pretreatments). Its cation exchange capacity was 67 cmol (+)/kg, its basal space 13.60 Å, its specific surface area 49 m^2/g, and its chemical composition (Table 1) led to the structural formula $[Si_{8.00}][Al_{2.717}Fe_{0.153}Mg_{1.206}Mn_{0.005}Ti_{0.026}]\ O_{20}(OH)_4\ [Ca_{0.262}Na_{0.017}K_{0.011}]$, which is a typical formula for a montmorillonite.

2.1.1. Synthesis of Si,Fe_x-Mt materials

The preparation of the Si,Fe_x-Mt materials was carried out adapting the method proposed by Avila et al. (2010). Purified montmorillonite (6.0 g) and distilled water (120 cm^3) were placed in a reaction flask under stirring, for 1 h, followed by the addition of the silylating agent (APTES, 2.4 cm^3, 10.26 mmol) and the definite amount of $FeCl_3{\cdot}6H_2O$ to reach Fe/Si atomic ratios of 6:94, 18:82 and 30:70, respectively. The dispersions were stirred at room temperature for 48 h. The solids were filtered, washed with toluene, dried under vacuum at 110 °C for 14 h, and calcined in air at 400 or 500 °C. The dried solids were designated as Si,Fe_6-Mt, Si,Fe_{18}-Mt and Si,Fe_{30}-Mt, respectively. The designation of the samples, and their chemical composition and textural data are presented in Tables 1–2.

2.1.2. Synthesis of Al,Fe_x-Mt materials

The preparation of the Al,Fe-Mt solids was carried out by pillaring, adapting the method proposed by Timofeeva et al. (2005). Montmorillonite (1% mass dispersion) was stirred in distilled water for about 24 h at 20 °C. At the same time, the Fe/Al solutions were prepared by mixing $AlCl_3{\cdot}6H_2O$ and $FeCl_3{\cdot}6H_2O$ (Al/Fe cationic ratios 12:1 and 11:2), with subsequent hydrolysis until pH = 4.3 using a Na_2CO_3 solution. Al/Fe solutions were added to the Mt at 80 °C and the mixture was stored overnight at room temperature. The intercalated solids were washed by centrifugation, dried in air at 70 °C, and calcined in air at 400 or 500 °C. The dried solids were designated as $Al_{12}Fe_1$-Mt and $Al_{11}Fe_2$-Mt, respectively. The designation of the samples, and their chemical composition and textural data are presented in Tables 1–2.

2.2. Instrumental measurements

Element chemical analyses were carried out at Activation Laboratories Ltd., in Ancaster, Ontario, Canada, using inductively coupled plasma-atomic emission spectrometry (ICP-AES). FT-IR spectra were recorded in the 450–4000 cm^{-1} range in a PerkinElmer Spectrum-One spectrometer by the KBr pellet method. X-ray diffraction (XRD) patterns were recorded between 2 and 65° (2θ) over non-oriented powder samples, at a scanning speed of 2°/min, by using a Siemens D-500 diffractometer, operating at 40 kV and 30 mA, and employing filtered Cu K_α radiation (λ = 1.5418 Å). Thermal analyses were conducted on a SDT Q600 TA instrument. All measurements were carried out under a flow of 20 cm^3/min of oxygen (Air Liquide, Spain, 99.999%) and a temperature heating rate of 10 °C/min from room temperature up to 900 °C.

Textural properties were determined from nitrogen (Air Liquide, 99.999%) adsorption data, obtained at − 196 °C using a Micrometrics

Table 1
Chemical composition of Si,Fe_x-Mt and Al,Fe_x-Mt materials.

	Chemical composition[a] (wt%)											
	SiO_2	Al_2O_3	Fe_2O_3	MnO	MgO	CaO	Na_2O	K_2O	TiO_2			
Mt	69.08	19.71	1.75	0.05	6.91	2.09	0.07	0.07	0.26			
										ΔSiO_2 (wt%)	ΔFe_2O_3 (wt%)	$\Delta Si/\Delta Fe$ (mol/mol)
Si,Fe_6-Mt	79.91	19.71	2.68	0.07	6.68	1.16	0.03	0.06	0.25	10.89	1.53	9.50
Si,Fe_{18}-Mt	79.90	19.71	4.22	0.08	6.47	0.52	0.03	0.05	0.26	10.88	2.47	5.87
Si,Fe_{30}-Mt	81.78	19.71	5.49	0.08	6.57	0.31	0.03	0.06	0.25	12.7	3.74	4.52
										ΔAl_2O_3 (wt%)	ΔFe_2O_3 (wt%)	$\Delta Al/\Delta Fe$ (mol/mol)
Al_{12},Fe_1-Mt	69.08	34.71	4.56	0.04	6.28	0.03	0.03	0.06	0.27	15.00	2.81	8.35
Al_{11},Fe_2-Mt	69.08	39.50	9.22	0.04	6.36	0.02	0.05	0.05	0.26	19.79	7.47	4.15

[a] Normalized composition (see Table S1).

Table 2
Textural properties of Si,Fe_x-Mt and Al,Fe_x-Mt materials.

	d_{001} (Å)	Textural properties			
		S_{BET} (m^2/g)	S_{ext} (m^2/g)	V_Σ (cm^3/g)	V_μ (cm^3/g)
Mt	13.60	49	49	0.070	0.001
Mt(500)	9.57	80	64	0.103	0.009
Si,Fe_6-Mt	13.69	1	0	–	–
Si,Fe_6-Mt(400)	12.93	9	8	0.015	0.001
Si,Fe_6-Mt(500)	13.89	138	49	0.103	0.049
Si,Fe_{18}-Mt	13.49	16	16	0.027	–
Si,Fe_{18}-Mt(400)	13.49	21	18	0.037	0.002
Si,Fe_{18}-Mt(500)	13.69	152	55	0.117	0.054
Si,Fe_{30}-Mt	13.89	18	18	0.031	–
Si,Fe_{30}-Mt(400)	13.30	35	27	0.049	0.005
Si,Fe_{30}-Mt(500)	13.69	171	58	0.129	0.063
Al_{12},Fe_1-Mt	15.26	181	72	0.134	0.060
Al_{12},Fe_1-Mt (400)	16.04	176	82	0.137	0.053
Al_{12},Fe_1-Mt (500)	15.26	167	80	0.133	0.049
Al_{11},Fe_2-Mt	14.44	141	77	0.137	0.036
Al_{11},Fe_2-Mt (400)	14.32	151	88	0.157	0.035
Al_{11},Fe_2-Mt (500)	13.89	134	77	0.147	0.031

Gemini VII 2390 t, Surface Area and Porosity apparatus. Specific surface area was obtained by the BET method (S_{BET}), external surface area (S_{ext}) and micropore volume (V_μ) by means of the t-method, and the total pore volume (V_Σ) from the nitrogen adsorbed at a relative pressure of 0.95 (Brunauer et al., 1938; Lippens and De Boer, 1965; Rouquerol et al., 1998; Lowell et al., 2010).

The DR-UV–vis spectra were recorded on a UV-2501 PC Shimadzu spectrometer with a IRS-250A accessory in the 190–900 nm range with a resolution of 2 nm, on samples in powder form placed into a special cell for DR-UV–vis measurement. $BaSO_4$ was used as standard for measurements. The DR-UV–vis spectra are presented in a form of Kubelka-Munk function (Kustov, 1997): $F(R) = \frac{(1-R)^2}{2R}$, where R is the reflection coefficient.

For surface acidity studies, the samples were pre-treated in oxygen at 400 °C for 1 h before the adsorption experiments. Then, the samples were loaded into the DR-IR cell and heated at 400 °C under vacuum for 1 h. After this activation, the samples were exposed to saturated pyridine vapours at room temperature for 10 min and under vacuum for 15 min at 150 °C. Then, pyridine was desorbed until a pressure of 10^{-6} mbar, when there was no more pyridine physisorbed on the wafers. DRIFT spectra were recorded with a FTIR-8400S Shimadzu spectrometer equipped with a DRS-8000 diffuse reflectance cell in the range of 400–6000 cm^{-1} with a resolution of 4 cm^{-1}. The strength of Brønsted acid sites (BAS) was characterized by the proton affinity values (PA) (Davydov, 2003).

2.3. Catalytic tests

The reaction of 1,2-phenylenediamine (**I**) with acetone was carried out at 50 °C in a glass reactor equipped with a magnetic stirrer. Methanol, acetonitrile and 1,2-dichloroethane were considered as solvents, and after a preliminary study (see below), methanol was selected for further experiments. Before reaction all catalysts were activated at 200 °C for 2 h in air in order to remove adsorbed water. The standard procedure was as follows: 0.1 mmol of (**I**), 4 cm^3 of solvent, 2.5–4 mmol of acetone and 5–20 mg of catalyst were added into the reactor. At several time intervals aliquots were taken from the reaction mixture transferred to the GC and GCMS analysis. A gas chromatograph (Agilent 7820) with a flame ionization detector and the capillary column HP-5 were used to analyze products quantitatively. The GCMS analysis of organic phase was performed with GCMS-QP2010 Ultra Gas chromatography mass spectrometer. Analysis conditions were as follows: GC: Injection port temperature 250 °C, capillary column GsBP1-MS 30 m × 0.32 mm, programmed heating: 50 °C (7.5 min) – 20 °C/min – 300 °C (10 min), carrier gas – He (linear velocity of 50 cm/s); MS: Determined *m/z* 35–500 detector voltage 0.8 kV, emission current 60 μA, ion source temperature 250 °C (MS data are given in Fig. S1, Supporting Information). The iron content in the solids after reaction was determined by atomic absorption analysis (AAS SolaarM 6 spectrometer).

3. Results and discussion

3.1. Characterization of Si,Fe_x-Mt and Al,Fe_x-Mt materials

3.1.1. Chemical analysis

Chemical analysis of Si,Fe_x-Mt materials (Tables 1 and S1–S3) were carried out on the solids after treatment with APTES and $FeCl_3$ via the sol-gel polymerization technique and calcination in air at 500 °C for the removal of the organic moieties. The incorporation of Si, Al and Fe to the Mt solids (Table S1) was carried out by cation exchange of the exchangeable Ca^{2+}. The normalized amount (Table 1) of SiO_2 inserted into the framework of Mt was 10.8–12.7 wt%; these amounts corresponded to 74–100% from the theoretical values (Table S2). The amount of Fe_2O_3 increased from 2.6 to 5.49 wt% with the Fe-content in the treating solutions, although decreasing at the same time the

percentage fixed with respect to the amount in the treating solutions (100 to 73%). It can be suggested that the intercalation of Mt by APTES mainly proceeded due to the interaction of –OH surface functional groups of Mt with APTES. At the same time, the incorporation of Fe_2O_3 occurred both via (a) cation exchange, i.e. the removal of exchangeable Ca^{2+}, and (b) complex formation with -NH_2 groups of APTES. The adsorption of Fe^{3+} on solids modified by APTES has been demonstrated in the literature (Moghimi, 2014; Basumatary et al., 2016). The estimation of the contribution from each process (Table S3) pointed out that both processes proceeded concurrently. The contribution from complex formation increased when all the exchangeable Ca^{2+} cations were substituted by Fe^{3+}. At the same time, Fe^{3+} could also bond to the surface of silica sol particles, in a similar way to the sol particles reported by Han et al. (Han et al., 1997; Han and Yamanaka, 1998) (although these authors hydrolyzed Si-ethoxide with HCl in ethanol or used large tetraalkylammonium cations in their synthesis, obtaining large sol particles), thus the increase of Fe^{3+} in the solutions favoured the formation of charged Fe^{3+}-SiO_2 sol particles, also favouring their incorporation to the solid by exchange of Ca^{2+} cation.

In the case of the pillared solids, the amounts of Al_2O_3 fixed were 15 and 20 wt% for Al_{12},Fe_1-Mt and Al_{11},Fe_2-Mt, respectively, while the amount of Fe_2O_3 increased 2.8 and 7.5% for the same solids. The amount of the cations was in excess with respect to the CEC of the clay, and thus 51 and 74% of the Al^{3+} cations in the pillaring solutions were fixed by the solids, while the percentage of fixed Fe^{3+} was higher, 74 and 98% of the initial amounts, respectively. If mixed Al,Fe-polycations were considered derived from pure Al_{13}-Keggin, $[Al_{13}O_4(OH)_{24}(H_2O)_{12}]^{7+}$, the incorporation of Fe^{3+} to the polycation should occur with a decrease of the amount of Al^{3+}, and the same tendency should be maintained when the polycations were incorporated into the solids. However, the presence of Fe^{3+} should alter the polymerization of Al^{3+}, very sensitive to pH variation, changing its polymerization degree, and consequently the number of polycations needed to compensate the exchangeable charge, while Fe^{3+} should at the same time polymerise itself, what made difficult to correlate the amount of both elements. In these solids, the incorporation of the polycations by cation exchange completely removed Ca^{2+}, and even a small decrease (ca 0.6%) in the amount of Mg^{2+}, what suggested that a small amount of this element should also be exchangeable, or more probably, that it was leached from the octahedral sheet by the intercalating solutions (although the solution was only slightly acidic, pH 4.3, octahedral Mg^{2+} is very sensible to acidic conditions (Vicente-Rodríguez et al., 1996)).

3.1.2. X-ray diffraction

For the Si,Fe_x-Mt materials, the dried solids were highly ordered (Figs. 1 and S2), and their basal spaces were 13.5–13.9 Å (Table 2), not depending on the amount of Fe in the treating solutions. The calcination at 400 or 500 °C produced a strong decrease in the intensity of the (001) reflection, showing a loss of large distance ordering, but the basal space remained practically constant, suggesting that the height of the Fe^{3+}-SiO_2 particles incorporated to the interlayer space did not change appreciably. No significant differences in basal space were caused by increasing the calcination temperature from 400 to 500 °C, although the diffractograms showed more baseline noise, suggesting a detriment in the structure.

For the $Al_{13-x}Fe_x$-Mt-Mt materials (pillared series) (Figs. 1 and S3, Table 2), the dried solids showed basal spaces of 15.26 and 14.44 Å, lower than the values usually reported for Al_{13}-Keggin intercalated montmorillonites, so the presence of Fe^{3+} should significantly affect the polymerization process in the conditions used. The calcination decreased the ordering of the solids but it did not change significantly the basal space for the $Al_{12}Fe_1$-Mt, but a slow decrease was observed with the calcination temperature for $Al_{11}Fe_2$-Mt series, in agreement with the lower thermal resistance of Fe-PILC compared to Al-PILC.

The reflections belonging to the in-layer reflections, independent of *c*-stacking, were recorded at the same positions for all the solids, indicating that the layers were not modified. No reflections different from those of montmorillonite; that is, belonging to other crystalline phases involving Si, Al and/or Fe, were observed.

3.1.3. DR-UV–vis study

Intercalation of Mt by APTES, $FeCl_3$ and the mixture APTES and $FeCl_3$, at 25 and 70 °C for 24 h, was investigated by DR-UV–vis spectroscopy. Experimental conditions of the treatments were close to those of Si,Fe_{30}-Mt preparation. The DR-UV–vis spectrum of Mt (Fig. S4) showed a strong absorption band at 255 nm and two weak bands at 360 and 503 nm, which can be assigned to the charge-transfer transitions (CT) from O^{2-} to metal and d-d transitions of impurity ions, such as Fe^{3+}, Ti^{4+} etc. (Lever, 1984; Jitianu et al., 2002; Shafia et al., 2015). Intercalation of APTES, $FeCl_3$ and their mixture at 25 °C led to the increase in the intensity of the bands at 360 and 503 nm and the appearance of a new weak band at 648 nm attributed to d-d transitions of impurity ions. Similar trends were observed in DR-UV–vis spectra of Mt modified at 70 °C. In both cases, the intensity of the band at 503 nm in the spectrum of Mt/APTES-$FeCl_3$ was lower than that of Mt/$FeCl_3$ that can be a circumstantial evidence of interaction between $FeCl_3$ and APTES. According to Jitianu et al. (2002), the band at 503–525 nm (d-d spin forbidden transfer to $^4T_{2g}$) should be detected to a lesser extent in contrast to another spin forbidden transition to $^4T_{1g}$ around 650 nm in the spectra of the Fe-containing materials prepared with TEOS. These bands and the shift of CT band were used as evidences of the

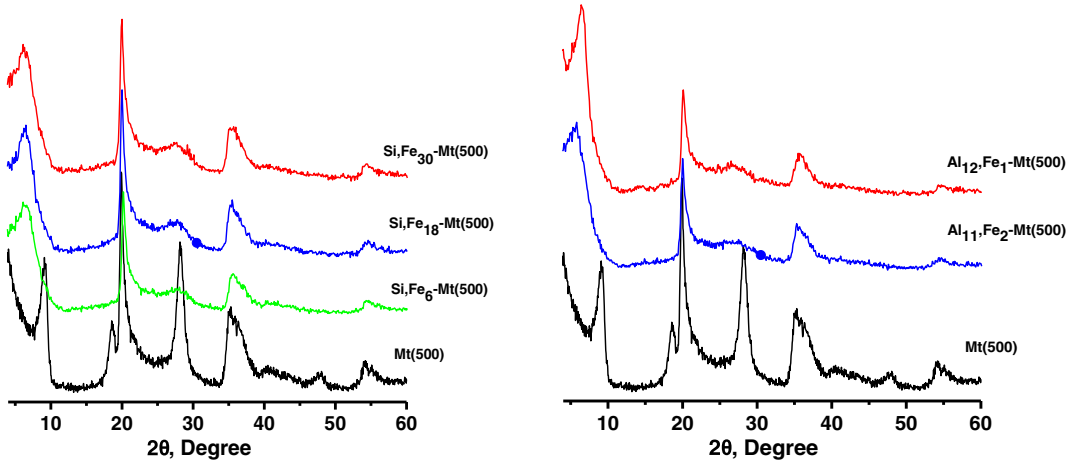

Fig. 1. XRD patterns of Si,Fe_x-Mt(500) and Al,Fe_x-Mt(500) materials.

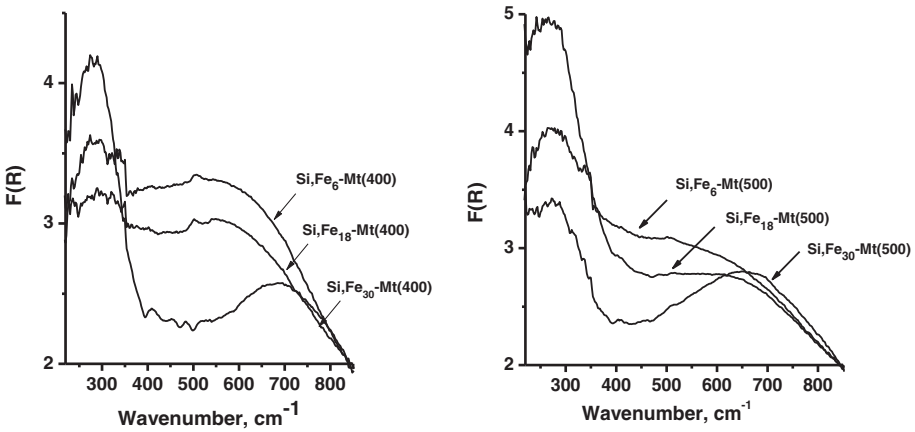

Fig. 2. DR-UV–vis spectra of Si,Fe_x-Mt and Al,Fe_x-Mt materials.

appearance of the iron ions involved in the chains −O−Si−O−⊕ Fe−O−Si−O−. Our experimental data pointed out that the modification of Mt at high temperature led to the shift of CT band from 225 to 272 nm. DR-UV–vis spectrum of Mt/APTES-$FeCl_3$ calcined at 500 °C was similar to the spectrum of Si,Fe_{30}-Mt (Fig. S4). The intensity of the band at 648 nm rose with the increasing of the temperature of Mt/APTES-$FeCl_3$ preparation. Therefore, all these changes in the spectra can point out to the insertion of reagents into the interlayer spacing of clay.

The state of iron in Si,Fe_x-Mt and $Al_{13-x}Fe_x$-Mt-Mt materials was studied by DR-UV–vis spectroscopy (Figs. 2 and S5). For all the samples, the DR-UV–vis spectra showed two strong absorptions with convoluted bands in a wavelength interval from 220 to 800 nm. Bands in the region below 300 nm were attributed to isolated Fe^{3+} sites in tetrahedral (228 nm) and higher coordination (290 nm) (Prieto et al., 1994; Fabrizioli et al., 2002). According to the literature, bands between 300 and 400 nm are assigned to octahedral Fe^{3+} in small oligomeric Fe_xO_y clusters, while bands above 450 nm can be ascribed to large Fe_2O_3 particles (Sherman, 1985; Jitianu et al., 2002). For Si,Fe_x-Mt samples, the state of iron was determined by the Fe content in the solids (Fig. 2); the intensity of the bands in the region of 300–450 nm strongly decreased with increasing Fe content from 1.88 to 3.87 wt%. This phenomenon can be related to the increasing amount of large Fe_2O_3 particles. Si,Fe_{30}-Mt had practically only large Fe_2O_3 particles in the framework.

The iron state also depended on the Fe content in Al,Fe_x-Mt series (Fig. S5). However, in contrast to Si,Fe_x-Mt materials, the intensity of the bands in the region of 250–450 nm was strongly higher than that of the bands above 450 nm. This difference indicated the larger amount of isolated Fe^{3+} sites and Fe^{3+} in small oligomeric Fe_xO_y clusters in comparison with large Fe_2O_3 particles.

3.1.4. IR study

The IR spectra of the treated samples (Fig. 3) were rather similar to that of raw montmorillonite. Stretching O−H and bending H−O−H water vibrational modes were recorded around 3433 and 1636 cm^{-1}, respectively, while stretching vibration of silica-oxygen tetrahedrons ν_{as}(Si−O−Si) was observed at 1111 cm^{-1} with a shoulder at 1036 cm^{-1}, and bending ν(Si−O) and stretching ν(M−O) vibrations were observed at 519 cm^{-1} (Kim and Ahn, 1991; Wu et al., 1998). The intensity of the O−H stretching mode of the hydroxyl groups bonded to the metals, recorded around 3621 and 3438 cm^{-1}, increased after the treatments, showing the creation of these groups in the surface of the Al/Fe pillars and of Fe−SiO_2 particles. Three weak bands at 914, 843 and 795 cm^{-1} related to stretching vibrations of M−O (M = Al, Fe, Mg) were sharper in the treated solids than in the raw Mt. In the Si−Fe series, the uncalcined solids showed clear C−H vibrations close to 2852 and 2928 cm^{-1}, and a band from NH_2-groups at 1512 cm^{-1}, that disappeared after calcination.

3.1.5. Thermogravimetric analysis

The thermogravimetric curves of the solids from Al,Fe_x-Mt series were similar to those from raw montmorillonite, with small differences due to the higher water content in the intercalated solids, associated to the polycations (Fig. S6). Mt had simple thermal curves, with two main effects, the loss at low temperature of water adsorbed on the surface and coordinated to the exchangeable cations (12% mass) and the dehydroxylation at high temperature (6% mass). For the Si,Fe-Mt series, curves from Si,Fe_6-Mt are given as example in Fig. 4, mass loss due to dehydration was observed as two overlapped effects in the TG curve, associated to an endothermic effect centred at 61 °C and a shoulder close to 180 °C in the DTA curve, the mass loss summing about 9%. An important mass loss was found in the central region of temperature, associated to an exothermal effect centred at 390 °C, reasonably due to

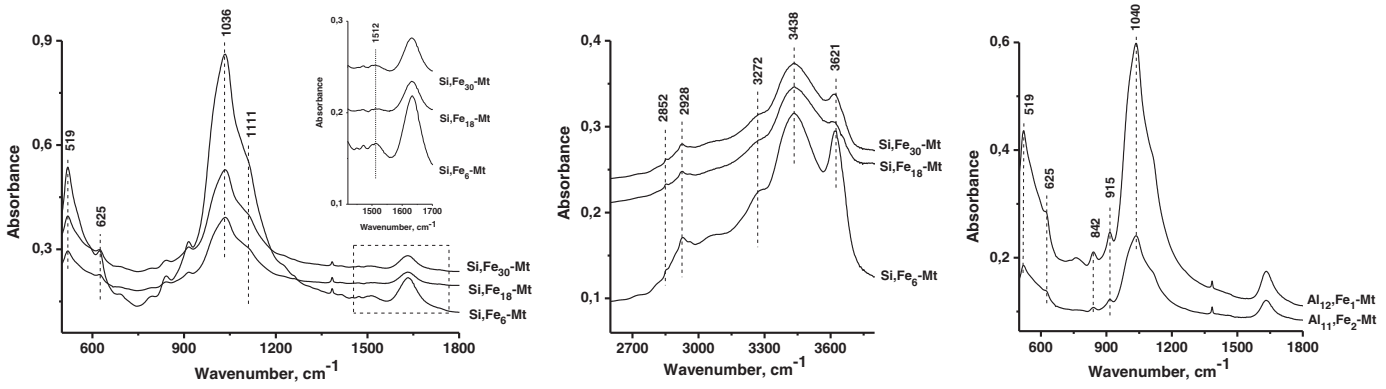

Fig. 3. FT-IR spectra of Si,Fe_x-Mt and Al,Fe_x-Mt materials before calcination.

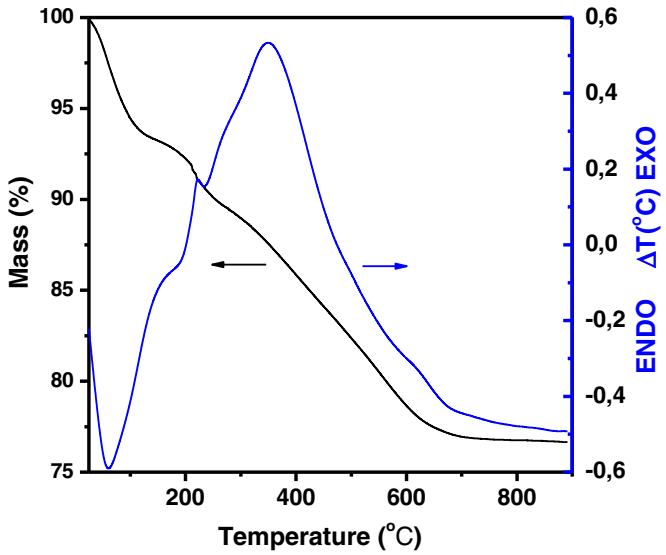

Fig. 4. Thermal curves (TG and DTA) of Si,Fe_2-Mt solid.

the removal of the organic matter from the silane that remained in the solid. The total mass loss increased in this series to almost 30% of the initial mass of the solids.

3.1.6. Textural properties

The nitrogen adsorption/desorption isotherms (Fig. 5 and S7) belonged to type II from IUPAC classification, with a H4 type hysteresis loop at high relative pressures, which is associated to narrow slit pores (Lowell et al., 2010). The loop had an inflexion at a relative pressure value of 0.4, being reversible at low p/p^0 values for all the solids. Raw Mt had a low S_{BET} value, 49 m^2/g (Table 2). This solid was calcined at 500 °C, under the same conditions used for the preparation of the pillared solids, and S_{BET} value increased to 80 m^2/g, attributable to the "cleaning" and thermal activation of the solid during calcination.

In the $SiFe_x$-Mt series, the dried solids showed very low S_{BET} values, between 1 and 18 m^2/g (Table 2), all being external surface area, suggesting that the interlayer space was almost completely occupied by the Fe—Si particles, which before calcination maintained organic moieties derived from APTES silane. The calcination at 400 °C produced a small increase of the S_{BET}, but the main part of the organic matter may still remain in the solids, blocking the access of the adsorbate to the interlayer space. The situation strongly changed when calcining at 500 °C, the organic matter should be mostly or completely eliminated, leading to solids with S_{BET} remarkably increased, to values between 138 and 171 m^2/g, being about 2/3 of the S_{BET} due to micropore surface, while micropore volume reached 0.05–0.06 cm^3/g and the total pore volume 0.10–0.13 cm^3/g. It is interesting to remark that if the magnitudes were compared among the three solids treated at the same temperature, they increased parallel to the amount of Fe incorporated to the solids.

In the Al-Fe series, the S_{BET} was very close for all the solids (Table 2). As indicated in XRD discussion, the basal space of the solids did not change significantly, so the access to the interlayer space was already possible for the dried solids, and did not significantly vary under calcination at 400 or 500 °C. Although it was expected that the calcination decreased the size of the intercalating species, transforming them from polycations to pillars and increasing the accessible interlayer space, this was probably compensated by the lower PILC stability induced by the presence of Fe. Thus, although the montmorillonite structure did not collapse, its ordering was lower, making difficult the access to the interlayer. S_{BET} thus reached 134–176 m^2/g, half of it being external surface area, and total porosity reaching 0.13–0.16 cm^3/g.

3.1.7. Surface acidity

Surface acidity of Si,Fe_x-Mt and Al_{12},Fe_1-Mt materials was analysed by IR spectroscopy using pyridine as probe molecule. Pyridine molecule can interact with both LAS and BAS (Kustov, 1997; Davydov, 2003). Thus, adsorption of pyridine on LAS leads to the appearance of an IR absorption band (a.b.) at 1445 cm^{-1}, while a.b. at 1540–1545 cm^{-1} is traditionally attributed to BAS due to the formation of pyridinium cations. Absorption bands at 1545 and 1445 cm^{-1} in the DRIFT spectra of Si,Fe_x-Mt and Al_{12},Fe_1-Mt materials after adsorption of pyridine (Fig. S8) pointed out the existence of BAS (H-bond donor sites formed by mainly isolated surface −OH groups) and LAS (sites formed by Fe^{3+} and Fe^{3+}/Al^{3+} cations), respectively. An a.b. at 1490 cm^{-1} was also observed in the spectra, assigned to pyridine adsorbed on both BAS and LAS, simultaneously (Parry, 1963). Therefore, the ratio of the integral intensities of I_{1455}/I_{1490} can give information on the change in the amount of LAS in the solids. In Si,Fe_x-Mt solids, I_{1455}/I_{1490} ratio rose with increasing Fe content (Fig. S9), which was also in agreement with the increasing integral intensity in this case of a.b. at 1445 cm^{-1}. The integral intensity of a.b. at 1540 cm^{-1} was higher in $Al_{12}Fe_1$-Mt solid than in Si,Fe_x-Mt ones, which can point out the larger amount of BAS in this solid compared to those of Si,Fe_x-Mt series. The strength of BAS was estimated using the method suggested by Paukshtis and Urchenko (1983). The variation of Fe content slightly affected the PA value (Table S4); the increase in Fe content from 1.88 to 3.87 wt% led to the increase in PA from 1199 to 1180 kJ/mol. The PA values for Si,Fe_{30}-Mt and Al_{12},Fe_1-Mt were similar, i.e. these samples possessed BAS with similar strength.

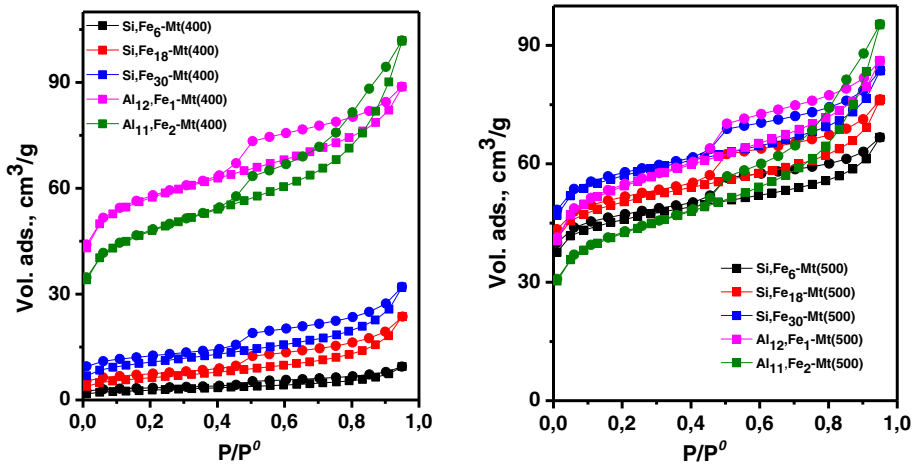

Fig. 5. Nitrogen adsorption–desorption isotherms of Si,Fe_x-Mt and Al,Fe_x-Mt materials.

Table 3
Effect of solvent on reaction of (I) with acetone in presence of Si,Fe_{30}-Mt(500).[a]

Solvent	Relative polarity[b]	Conversion of (I) (%)	Selectivity (%)		
			(II)	(III)	(Other)
Methanol	0.672	90.2	33.7	58.6	7.7
Acetonitrile	0.460	44.4	81.5	3.8	14.7
1,2-Dichloroethane	0.269	36.3	87.3	2.5	10.2

[a] Reaction conditions: 0.1 mmol of (I), 0.25 mmol of acetone, 0.015 g of catalyst, 4 cm^3 of solvent, 50 °C, 90 min.
[b] Data from (Reichardt, 2003).

3.2. Catalytic properties of Si,Fe_x-Mt and Al,Fe_x-Mt materials

Catalytic properties of Si,Fe_x-Mt and Al,Fe_x-Mt materials were studied in the reaction of (I) with acetone, at a acetone/(I) molar ratio of 2.5 and 50 °C. The catalytic properties of Si,Fe_{30}-Mt(500) were investigated in methanol, acetonitrile and 1,2-dichloroethane, because the reaction rate and the yield of (III) can depend on the polarity of the solvent (Pawar et al., 2009; Sagar et al., 2013). The decreasing of solvent polarity (relative polarity (Reichardt, 2003)) led to the decrease in the conversion of (I) and yield of (III) (Table 3). Maximal yield of (III) (52.9%) was observed in methanol with large relative polarity (0.672). The effect of the solvent polarity seemed to be related to the formation and the spatial arrangement of the intermediates; thus, methanol was selected as the reaction medium for the following investigations.

All Si,Fe_x-Mt and Al,Fe_x-Mt materials showed high catalytic performance (Table 4). The reaction had heterogeneous character in the presence of Si,Fe_x-Mt and Al,Fe_x-Mt materials calcined at 500 °C that was confirmed by the experiments after removal of catalysts by filtration. Thus, the Si,Fe_6-Mt sample was filtered off after 15 min of reaction, where the conversion of (I) was about 42.6%. Then, the filtrate without the catalyst was stirred at 50 °C for 30 min. Conversion of (I) was 43.8%. This result suggested that the reaction could not proceed in the absence of a catalyst. Moreover, leaching of Fe from Si,Fe_x-Mt samples was not detected by atomic absorption analysis. On the opposite, leaching of Fe from the solids to the reaction medium was observed in the presence of Si,Fe_x-Mt and Al,Fe_x-Mt materials calcined at 400 °C, which suggested that the stabilization of Fe-species was not complete after calcination at this temperature. The presence of Fe in the reaction mixture seemed to be responsible of the higher conversion of (I) and selectivity towards (III) in the presence of these samples in comparison with Si,Fe_x-Mt and Al,Fe_x-Mt materials calcined at 500 °C, by means of homogeneous contribution to the reaction. Thus, Si,Fe_x-Mt and Al,Fe_x-Mt materials calcined at 500 °C were preferred for the following investigations.

Table 4
Catalytic properties of Si,Fe_x-Mt and Al,Fe_x-Mt materials in the cyclocondensation of (I) with acetone.[a]

	Time (min)	Leaching of Fe[b] (wt%)	Conversion of (I) (%)	Selectivity (%)		
				(II)	(IIa)	(III)
Without catalyst	90	–	< 1	100	n.d.	n.d.
Mt(500)	90	–	5.2	91.2	8.8	n.d
Si,Fe_6-Mt	10		14.7	85.8	13.1	1.1
(400)	90	13.8	93.2	35.2	8.7	56.1
Si,Fe_{18}-Mt	10		34.9	80.8	17.8	2.0
(400)	90	13.9	96.9	20.2	7.6	72.2
Si,Fe_{30}-Mt	10		44.3	79.7	16.8	3.3
(400)	90	15.3	97.1	20.0	6.9	73.1
Al_{12},Fe_1-Mt	10		56.6	78.9	15.1	6.0
(400)	90	3.5	95.6	32.0	0.1	67.9
Si,Fe_6-Mt	10		18.3	94.9	0.1	5.0
(500)	90	n.d.	75.1	53.2	10.3	36.5
Si,Fe_{18}-Mt	10		30.9	97.5	0.0	2.5
(500)	90	n.d.	89.1	32.2	7.1	60.7
Si,Fe_{30}-Mt	10		40.0	84.8	12.2	3.0
(500)	90	n.d.	90.2	33.7	7.7	58.6
Al_{12},Fe_1-Mt	10		52.7	76.4	17.4	6.2
(500)	90	n.d.	93.1	32.0	7.6	60.4

[a] Reaction conditions: 0.1 mmol of (I), 0.25 mmol of acetone, 0.015 g of catalyst, 4 cm^3 of MeOH, 50 °C.
[b] Leaching of Fe based on the content of this element in each solid.

The kinetic curves in the presence of Si,Fe_x-Mt and Al,Fe_x-Mt materials calcined at 500 °C (Fig. S10) indicated that the reaction proceeded via two steps (Scheme 1). Thus, the product (II) was formed from (I) and one molecule of acetone in the first step reaction, and the posterior reaction between (II) and a second molecule of acetone led to the formation of product (III).

Conversion of (I) and yields of (II) and (III) depended on the Fe content in the solids. The reaction rate and yields of (II) and (III) rose linearly with the increasing of Fe content in Si,Fe_x-Mt materials (Fig. 6). The comparison of the catalytic properties of the solids with similar Fe content, i.e. Si,Fe_{30}-Mt(500) and Al_{12},Fe_1-Mt(500), pointed out that the efficiency of the pillared solid was higher than that of the sol-gel one. The higher performance of Al_{12},Fe_1-Mt(500) can be explained by the increasing amount of Lewis acid sites that followed from the data of IR spectroscopy using pyridine as probe molecule; conversion of (I) and yields of (II) and (III) followed linear trends with respect to I_{1455}/I_{1490} ratio (Fig. 7). The kinetic curves and the effect of Fe content on the reaction were in agreement with the reaction mechanism of cyclocondensation of 1,2-phenylenediamines with ketones (Fazaeli and Aliyan, 2007; Climent et al., 2009; Yadav and Yadav, 2013). It can be assumed that both acetone and (**I**) coordinate on the LAS, simultaneously, and the interaction of acetone with LAS led to the activation of the carbonyl group. Then the NH_2-groups of (**I**) attacked the carbonyl group of the acetone, giving the intermediate **1**

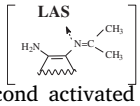

which can attack the carbonyl group of a second activated acetone molecule giving diimine,

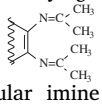

which after intramolecular imine enamine cyclization formed the seven-membered 1,5-benzodiazepine ring. Moreover, intermediate **1** can transform to dihydrobenzoimidazole (**IIa**) due to the inside cyclization.

The efficiency of Si,Fe_{30}-Mt and Al_{12},Fe_1-Mt materials was compared with that of Fe-containing materials, such as Fe-containing microporous nickel phosphate molecular sieves (6.5%Fe-VSB-5) and Fe-containing mesoporous mesophase silica material (1.7%Fe-MMM) (Timofeeva et al., 2017) and metal-organic framework MIL-100(Fe), and zeolites, such as HY (Si/Al 2.5, framework type FAU) heulandite (Si/Al 5, framework type HEU), H-ZSM-5 (Si/Al 28, framework type MFI) and β-zeolite (Si/Al 30, framework type BEA) (Tajbakhsh et al., 2006; Timofeeva et al., 2017). The catalytic efficiency was compared at a 4/1 M ratio of acetone/(I), 0.2/1.0 mass ratio of catalyst/(I) and 50 °C under solvent free conditions (Table 5). After 300 min, both Si,Fe_{30}-Mt and Al_{12},Fe_1-Mt materials led to yields of (III) higher than those obtained in the presence of microporous 6.5%Fe-VSB-5 (Table 5, runs 2, 4 and 5). At the same time, the efficiencies of mesoporous 1.7%Fe-MMM, MIL-100(Fe) and HY with small amount of mesopores were higher than those of Si,Fe_{30}-Mt and Al_{12},Fe_1-Mt materials (Table 5, runs 2, 4 and 6–8), that can be related to the difference in accessibility to the active sites for the reactants. Probably, the high microporosity of Si,Fe_{30}-Mt and Al_{12},Fe_1-Mt materials obstructed the free passage of (I) and the reaction products. Remarkably, the efficiencies of these materials were larger than those of H-ZSM-5 and β-zeolite (Table 5, runs 2, 4 and

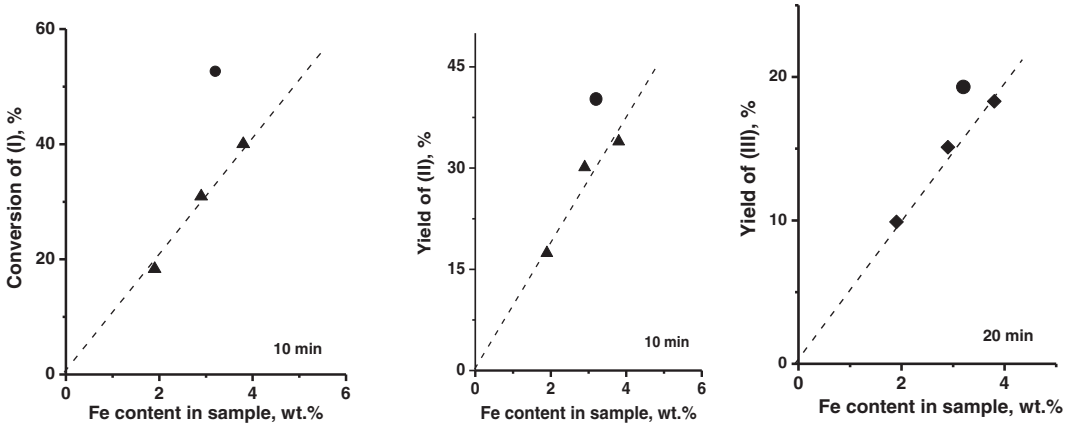

Fig. 6. Effect of the Fe content in Si,Fe_x-Mt and Al_{12},Fe_1-Mt materials calcined at 500 °C on the conversion of (**I**) and yield of (**II**) for 10 min and yield of (**III**) for 20 min in the reaction of cyclocondensation of (**I**) with acetone (Reaction conditions: 0.1 mmol of (**I**), 0.25 mmol of acetone, 0.015 g of catalyst, 4 cm^3 of solvent, 50 °C) (▲ - Si,Fe_x-Mt(500) materials; ● - Al_{12},Fe_1-Mt(500) materials).

10–12). The high surface acidity of Al_{12},Fe_1-Mt contributed to the high yield of (III), which was similar to that found in the presence of heulandite (Table 5, runs 4 and 9).

4. Conclusions

Fe-containing materials based on montmorillonite were prepared by two approaches, namely the pillaring method with Keggin type mixed $Al_{13-x}Fe_x$-polycations (x = 1, 2), and the sol-gel polymerization using 3-aminopropyltriethoxysilane (APTES) and $FeCl_3$ as sources of Si and Fe, with Fe atomic percentages x = 6, 18 and 30%, in aqueous medium. Two series of Fe-containing materials, Al_{13-x},Fe_x-Mt and Si,Fe_x-Mt, were thus prepared. In the sol-gel procedure, the incorporation of Fe and Si in the interlayer space of the clay mineral proceeded via (a) cation exchange of exchangeable Ca^{2+}, (b) complex formation with $-NH_2$ groups of APTES, and (c) the formation of charged Fe^{3+}-SiO_2 sol particles. Specific surface area of Si,Fe_x-Mt samples depended on the calcination temperature and was high (138–171 m^2/g) after calcination at 500 °C. Fe content in the samples affected their specific surface area and interlayer distance, and the oligomeric state of Fe species, the specific surface area rose from 138 to 171 m^2/g with increasing of Fe content from 1.9 to 3.8 wt%, while the larger Fe content, the larger particle size of Fe_2O_3.

Catalytic properties of Si,Fe_x-Mt and Al_{13-x},Fe_x-Mt materials were investigated in cyclocondensation of 1,2-phenylenediamine (I) with acetone to 1,5-benzodiazepine at 50 °C, with the acetone/(I) molar ratio of 2.5 in different solvent medium (methanol, acetonitrile, 1,2-dichloroethane) and under solvent free conditions. The yield of 1,5-benzodiazepine decreased in the order: methanol > acetonitrile > 1.2-dichloroethane, in agreement with the decreasing of solvent polarity.

Si,Fe_x-Mt samples calcined at 400 °C possessed low stability towards leaching of Fe, Fe-species were not fully stabilized at this temperature. The reaction rate and yield of (III) depended on the Fe content in Si,Fe_x-Mt(500). The increasing Fe content led to the rise of the reaction rate

Table 5
Reaction of 1,2-phenylenediamine with acetone in the presence of several catalytic systems.[a]

	Catalyst	Time (min)	Yield of (III) (%)	Ref.
1	Si,Fe_{30}-Mt(500)	210	65	This work
2		300	73	This work
3	Al_{12},Fe_1-Mt(500)	210	72	This work
4		300	80	This work
5	6.5%Fe-VSB-5	300	64	Timofeeva et al., 2017
6	1.7%Fe-MMM	300	86	Timofeeva et al., 2017
7	MIL-100(Fe)	180	76 (88)[b]	This work
8	HY	180	82	Tajbakhsh et al., 2006
9	Heulandite	300	81	Tajbakhsh et al., 2006
10	β-zeolite	300	39	Timofeeva et al., 2017
11	H-ZSM-5	300	32	Timofeeva et al., 2017
12	H-ZSM-5	420	52	Tajbakhsh et al., 2006

[a] 0.1 mmol of (I), 0.4 mmol of acetone, 0.02 g of catalyst, 50 °C.
[b] Yield of (III) after 5 h.

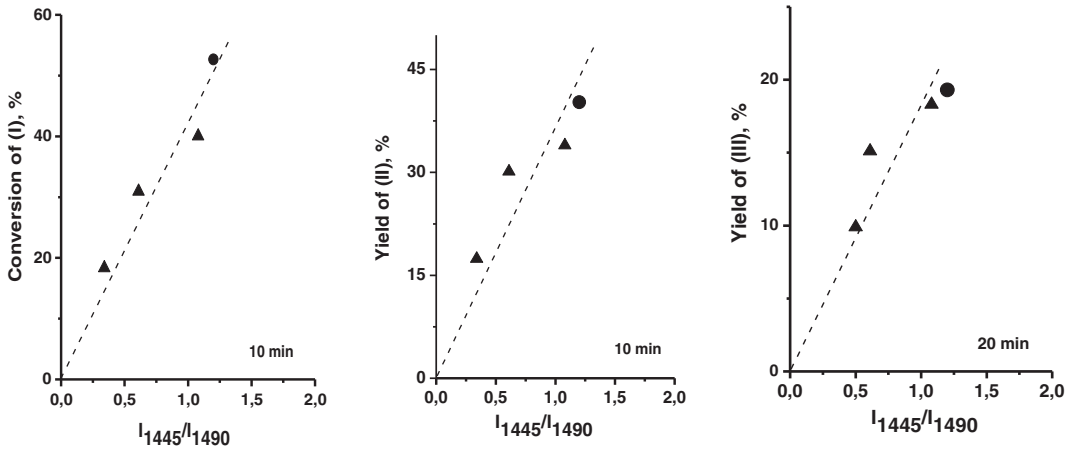

Fig. 7. Effect of LAS/(LAS + BAS) ratio in Si,Fe_x-Mt and Al_{12},Fe_1-Mt materials calcined at 500 °C on the conversion of (**I**) and yield of (**II**) for 10 min and yield of (**III**) for 20 min in the reaction of cyclocondensation of (**I**) with acetone (Reaction conditions: 0.1 mmol of (**I**), 0.25 mmol of acetone, 0.015 g of catalyst, 4 cm^3 of solvent, 50 °C) (▲ - Si,Fe_x-Mt(500) materials; ● - Al_{12},Fe_1-Mt(500) materials).

and yield of (III). Catalytic performance of Al_{12},Fe_1-Mt with 3.2 wt% of Fe was higher than that of Si,Fe_{30}-Mt with 3.8 wt%, explained by the difference in surface acidity. Efficiencies of Al_{12},Fe_1-Mt were lower than those of other mesoporous materials, and higher than those of other microporous materials.

Acknowledgments

This work was conducted within the framework of the budget project No. 0303-2016-0007 from the Boreskov Institute of Catalysis, and the research project MAT2013–47811–C2–R, jointly financed from the Spanish Agencia Estatal de Investigación, AEI (Spanish Ministry of Economy and Competitiveness, MINECO) and the European Regional Development Fund, ERDF.

Appendix A. Supplementary data

Supplementary data to this article can be found online at http://dx.doi.org/10.1016/j.clay.2017.06.028.

References

Avila, L.R., de Faria, E.H., Ciuffi, K.J., Nassar, E.J., Calefi, P.S., Vicente, M.A., Trujillano, R., 2010. New synthesis strategies for effective functionalization of kaolinite and saponite with silylating agents. J. Colloid Interface Sci. 341, 186–193.

Basumatary, A.K., Kumar, R.V., Ghoshal, A.K., Pugazhenthi, G., 2016. Removal of $FeCl_3$ from aqueous solution by ultrafiltration using ordered mesoporous MCM-48 ceramic composite membrane. Sep. Sci. Technol. 51, 2038–2046.

Bennamane, N., Kaoua, R., Hammal, L., Nedjar-Kolli, B., 2008. Synthesis of new amino-1,5-benzodiazepine and benzotriazole derivatives from dimedone. Org. Commun. 1, 62–68.

Bergaya, F., Lagaly, G., 2013. Handbook of Clay Science, Second edition. Elsevier.

Brunauer, S., Emmet, P.H.E., Teller, E., 1938. Adsorption of gases in multimolecular layers. J. Am. Chem. Soc. 20, 1553–1564.

Chari, M.A., Syamasunder, K., 2005. Polymer (PVP) supported ferric chloride: an efficient and recyclable heterogeneous catalyst for high yield synthesis of 1,5-benzodiazepine derivatives under solvent free conditions and microwave irradiation. Catal. Commun. 6, 67–70.

Climent, M.J., Corma, A., Iborra, S., Santos, L.L., 2009. Multisite solid catalyst for cascade reactions: the direct synthesis of benzodiazepines from nitro compounds. Chem. Eur. J. 15, 8834–8841.

Davydov, A.A., 2003. Molecular Spectroscopy of Oxide Catalyst Surfaces. Wiley.

Essaber, M., Baouid, A., Hasnaoui, A., Benharref, A., Lavergne, J.P., 1998. Synthesis of new tri- and tetraheterocyclic systems: 1,3-dipolar cycloaddition of nitrilimines on 2,7-dimethyl-4-phenyl-3H-1,5-benzodiazepine. Synth. Commun. 28, 4097–4104.

Fabrizioli, P., Bürgi, T., Burgener, M., Doorslaer, S.V., Baiker, A., 2002. Synthesis, structural and chemical properties of iron oxide-silica aerogels. J. Mater. Chem. 12, 619–630.

Fazaeli, R., Aliyan, H., 2007. Clay (KSF and K10)-supported heteropoly acids: friendly, efficient, reusable and heterogeneous catalysts for high yield synthesis of 1,5-benzodiazepine derivatives both in solution and under solvent-free conditions. Appl. Catal. A-Gen. 331, 78–83.

Gil, A., Vicente, M.A., Korili, S.A., Trujillano, R., 2010. Pillared Clays and Related Catalysts. Springer.

Han, Y.S., Yamanaka, S., 1998. Preparation and adsorption properties of mesoporous pillared clays with silica sol. J. Porous. Mater. 5, 111–119.

Han, Y.S., Matsumoto, H., Yamanaka, S., 1997. Preparation of new silica sol-based pillared clays with high surface area and high thermal stability. Chem. Mater. 9, 2013–2018.

Jitianu, A., Crisan, M., Meghea, A., Rau, I., Zaharescu, M., 2002. Influence of the silica based matrix on the formation of iron oxide nanoparticles in the Fe_2O_3-SiO_2 system, obtained by sol-gel method. J. Mater. Chem. 12, 1401–1407.

Kaur, R.J., Gagandeep, K., 2013. Silicotungstic acid in organic synthesis: synthesis of 1,5-benzodiazepines and β-amino carbonyl compounds. Res. J. Chem. Sci. 3, 59–64.

Kim, G.J., Ahn, W.S., 1991. Direct synthesis and characterization of high-SiO_2-content mordenites. Zeolites 11, 745–750.

Kustov, L.M., 1997. New trends in IR-spectroscopic characterization of acid and basic sites in zeolites and oxide catalysts. Top. Catal. 4, 131–144.

Lever, A.B.P., 1984. Inorganic Electronic Spectroscopy. 480 Elsevier, Amsterdam.

Lippens, B.C., De Boer, J.H., 1965. Studies on pore systems in catalysis. J. Catal. 4, 319–323.

Lowell, S., Shields, J., Thomas, M.A., Thommes, M., 2010. Characterization of Porous Solids and Powders: Surface Area, Pore Size and Density. Springer.

Moghimi, A.L.I., 2014. Solid phase extraction of Cu(II), Fe(III) and Pb(II) ions nano-graphene with aminopropyltriethoxysilane (APTES)I. J. British 1, 11–18.

Moreira, M.A., Ciuffi, K.J., Rives, V., Vicente, M.A., Trujillano, R., Gil, A., Korili, S., de Faria, E.H., 2017. Effect of chemical modification of palygorskite and sepiolite by 3-aminopropyl triethoxisilane on adsorption of cationic and anionic dyes. Appl. Clay Sci. 135, 394–404.

Nabih, K., Baouid, A., Hasnaoui, A., Kenz, A., 2004. Highly regio- and diastereoselective 1,3-dipolar cycloaddition of nitrile oxides to 2,4-dimethyl-3H-1,5-benzodiazepines: synthesis of bis[1,2,4-oxadiazolo][1,5]benzodiazepine derivatives. Synth. Commun. 34, 3565–3572.

Parry, E.P., 1963. An infrared study of pyridine adsorbed on acidic solids. Characterization of surface acidity. J. Catal. 2, 371–379.

Pasha, M.A., Jayashankara, V.P., 2006. Synthesis of 1, 5-benzodiazepine derivatives catalysed by zinc chloride. Heterocycles 68, 1017–1023.

Paukshtis, E.A., Urchenko, E.N., 1983. Study of the acid-base properties of heterogeneous catalysts by infrared spectroscopy. Russ. Chem. Rev. 52, 242–258.

Pawar, S.S., Shingare, M.S., Thore, S.N., 2009. Novel, efficient, and green procedure for the synthesis of 1,5-benzodiazepines catalyzed by $MgBr_2$ in aqueous media. Chin. Chem. Lett. 20, 32–36.

Prieto, M.C., Amores, J.M.G., Escribano, V.S., Busca, G., 1994. Characterization of co-precipitated Fe_2O_3-Al_2O_3 powders. J. Mater. Chem. 4, 1123–1130.

Reddy, B.M., Sreekanth, P.M., 2003. An efficient synthesis of 1,5-benzodiazepine derivatives catalyzed by a solid superacid sulfated zirconia. Tetrahedron Lett. 44, 4447–4449.

Reichardt, C., 2003. Solvents and Solvent Effects in Organic Chemistry, 3rd ed. Wiley.

Rouquerol, F., Rouquerol, J., Sing, K., 1998. Adsorption by Powders and Porous Solids – Principles, Methodology and Applications. Academic Press.

Sagar, A.D., Tigote, R.M., Haval, K.P., Sarnikar, Y.P., Khapate, S., 2013. Mild and efficient phosphonitrilic chloride mediated synthesis for 1,5-benzodiazepines. IJSRP 3, 2250–3153.

Schutz, H., 1982. Benzodiazepines: A Handbook. Basic Data, Analytical Methods, Pharmacokinetics and Comprehensive Literature. Springer.

Shafia, E., Esposito, S., Manzoli, M., Chiesa, M., Tiberto, P., Barrera, G., Bonelli, B., 2015. Al/Fe isomorphic substitution versus Fe_2O_3 clusters formation in Fe-doped aluminosilicate nanotubes (imogolite). J. Nanopart. Res. 17, 336.

Sherman, D.M., 1985. The electronic structures of Fe^{3+} coordination sites in iron oxides: applications to spectra, bonding, and magnetism. Phys. Chem. Miner. 12, 161–175.

Tajbakhsh, M., Heravi, M.M., Mohajerani, B., Ahmadia, A.N., 2006. Solid acid catalytic synthesis of 1,5-benzodiazepines: a highly improved protocol. J. Mol. Catal. A-Chem. 247, 213–215.

Timofeeva, M.N., Mel'gunov, M.S., 2009. Design and application of iron-containing Mesoporous molecular sieves for peroxide oxidation of pollutants: effect of iron environment on textural, physicochemical and catalytic properties. In: Burness, L.T. (Ed.), Mesoporous Materials. Nova Science Publishers, pp. 1–28.

Timofeeva, M.N., Khankhasaeva, S.Ts., Badmaeva, S.V., Chuvilin, A.L., Burgina, E.B., Ayupov, A.B., Panchenko, V.N., Kulikova, A.V., 2005. Synthesis, characterization and catalytic application for wet oxidation of phenol of iron-containing clays. Appl. Catal. B–Environ. 59, 243–248.

Timofeeva, M.N., Malyshev, M.E., Panchenko, V.N., Shmakov, A.N., Potapov, A.G., Mel'gunov, M.S., 2010. $FeAl_{12}$-Keggin type cation as an active site source for Fe,Al-silica mesoporous catalysts. Appl. Catal. B–Environ. 95, 110–119.

Timofeeva, M.N., Prikhod'ko, S.A., Makarova, K.O., Malyshev, M.E., Panchenko, V.N., Ayupov, A.B., Jhung, S.H., 2017. Iron-containing materials as catalysts for synthesis of 1,5-benzodiazepine from 1,2-phenylenediamine and acetone. React. Kinet. Mech. Catal.. http://dx.doi.org/10.1007/s11144-017-1190-2. (in the press).

Vicente, M.A., Gil, A., Bergaya, F., 2013. Pillared clays and clay minerals. In: Bergaya, F., Lagaly, G. (Eds.), Handbook of Clay Science, Second edition. Part A: Fundamentals Elsevier, pp. 523–557.

Vicente-Rodríguez, M.A., Suárez, M., Bañares-Muñoz, M.A., López-González, J.D., 1996. Comparative FT-IR study of the removal of octahedral cations and structural modifications during acid treatment of several silicates. Spectrochim. Acta A 52, 1685–1694.

Wayde, B.P., Martens, N., Frost, R.L., 2011. Organosilane grafted acid-activated beidellite clay for the removal of non–ionic alachlor and anionic imazaquin. Appl. Surf. Sci. 257, 5552–5558.

Wu, P., Komatsu, T., Yashima, T., 1998. Isomorphous substitution of Fe^{3+} in the framework of aluminosilicate mordenite by hydrothermal synthesis. Microporous Mesoporous Mater. 20, 139–147.

Xu, J.X., Wu, H.T., Jin, S., 1999. Cycloaddition of benzoheteroazepine II. Reactions and conformations of cycloadducts on 1, 5-benzothiazepines and 1,5-benzodiazepines with nitrile imine and nitrile oxides. Chin. J. Chem. 17, 84–91.

Yadav, G.D., Yadav, A.R., 2013. Selective green synthesis of 1,5-benzodiazepine over modified heteropolyacid as nanocatalyst: kinetics and mechanism. Ind. Eng. Chem. Res. 52, 17812–17820.

Yadav, J.S., Reddy, B.V.S., Praveenkumar, S., Nagaigh, K., 2005. Indium(III) bromide: a novel and efficient reagent for the rapid synthesis of 1,5-benzodiazepines under solvent-free conditions. Synthesis 480–484.

Supporting Information

Two synthesis approaches of Fe-containing intercalated montmorillonites: Differences as acid catalysts for the synthesis of 1,5-benzodeazepine from 1,2-phenylenediamine and acetone

Beatriz González[1], Raquel Trujillano[1], Miguel A. Vicente[1*], Antonio Gil[2], Valentina N. Panchenko[3,4], Ekaterina Petrova[4], Maria N. Timofeeva[3,4* *]

[1]*Department of Inorganic Chemistry, University of Salamanca, Salamanca, Spain*

[2]*Department of Applied Chemistry, Public University of Navarra, 31006 Pamplona, Spain*

[3] *Boreskov Institute of Catalysis SB RAS, Prospekt Akad. Lavrentieva 5, 630090, Novosibirsk, Russian Federation*

[4] *Novosibirsk State Technical University, Prospekt K. Marksa 20, 630092, Novosibirsk, Russian Federation*

Corresponding authors

Miguel A. Vicente

Tel: +34-670-558-392

Fax: + 34-923-294-514

E-mail: mavicente@usal.es

Address: Departamento de Química Inorgánica, Universidad de Salamanca, Plaza de la Merced, S/N, E-37008 Salamanca, Spain

M.N. Timofeeva

Tel.: +7-383-330-7284

Fax: +7-383-330-8056

E-mail: timofeeva@catalysis.ru

Address: Boreskov Institute of Catalysis SB RAS, Prospekt Akad. Lavrentieva 5, 630090, Novosibirsk, Russian Federation

Table S1. Chemical composition of catalysts based on natural clay.

	Chemical composition (wt.%)								
	SiO_2	Al_2O_3	Fe_2O_3	MnO	MgO	CaO	Na_2O	K_2O	TiO_2
Mt	55.80	15.92	1.41	0.04	5.58	1.69	0.06	0.06	0.21
Si,Fe_6-Mt	57.65	14.22	1.93	0.05	4.82	0.84	0.02	0.04	0.18
Si,Fe_{18}-Mt	58.25	14.37	3.08	0.06	4.72	0.38	0.02	0.04	0.19
Si,Fe_{30}-Mt	57.55	13.87	3.86	0.06	4.62	0.22	0.02	0.04	0.18
Al_{12},Fe_1-Mt	45.76	22.99	3.02	0.03	4.16	0.02	0.02	0.04	0.18
Al_{11},Fe_2-Mt	41.73	23.86	5.57	0.02	3.84	0.01	0.03	0.03	0.16

The amount of water in the solids was rather different, the sum of the metal oxides varying between 75 and 81%, avoiding a direct comparison of the amount of Al_2O_3 and Fe_2O_3 fixed by the solids. To evidence such modifications, a double normalization was carried out: first, the amount of the metal oxides was normalized to a total of 100%, thus avoiding the presence of water (water-free solids), and secondly, an internal reference, which remained constant during the treatments, was looked for in the solids. For Al,Fe_x-Mt solids, SiO_2 -the usual reference- was used, assuming that the tetrahedral sheet was not altered by the pillaring. However, the silylation treatment produced the fixation of SiO_2 and this compound could not be used as internal standard, Al_2O_3 being used in this case. Normalized results are given in Table 1 (see text).

Table S2. Amount of SiO_2 inserted into Mt. [a]

	ΔSiO_2 (wt.%) [b]	ΔSiO_2 (g)	% from theoretical [c]
Si,Fe_6-Mt	10.83	0.1083	86
Si,Fe_{18}-Mt	10.82	0.1082	86
Si,Fe_{30}-Mt	12.70	0.1270	100

[a] All results are referred to normalized composition, that is, to the composition given in Table 1.

[b] Referred to 100 g of dry raw montmorillonite (sample Mt in Table 1).

[c] Theoretical value of SiO_2 that can be fixed per gram of dry montmorillonite = 0.1253 g (considering the treatment carried out, 2.4 cm^3 of APTES per 6 g of natural clay).

Table S3. Chemical composition of catalysts based on natural clay.

	Experimental data					CC_{Ca}^{Fe} [b] (mmol/g)	ΔFe^{3+}(Other) [c] (mmol/g)
	ΔFe^{3+}		Amount of Ca^{2+}		ΔCa^{2+} [a]		
	(wt.%)	(mmol/g)	(wt.%)	(mmol/g)	(mmol/g)		
Si,Fe_6-Mt	1.85	0.34	0.83	0.21	0.16 (43.2%)	0.11	0.23
Si,Fe_{18}-Mt	2.45	0.52	0.37	0.09	0.28 (75.7%)	0.19	0.33
Si,Fe_{30}-Mt	1.75	0.68	0.22	0.05	0.32 (86.5%)	0.21	0.47

[a] Amount of Ca in Mt was 1.49 wt.% (0.37 mmol/g).

[b] Cation exchange: Amount of Fe^{3+} based on ΔCa^{2+}. CC_{Ca}^{Fe} is amount of Fe^{3+} which substituted Ca^{2+} leached from Mt (2 mol of Fe^{3+} to 3 mol of Ca^{2+}).

[c] Amount of Fe^{3+} forming complexes with -NH_2 groups of APTES and adsorbed on SiO_2-particles.

Table S4. Surface acidity of Si,Fe_x-Mt and Al,Fe_x-Mt materials.

	PA (kJ/mol)	LAS/(LAS+BAS) (a.u./a.u.)
Si,Fe_6-Mt	1199	0.34
Si,Fe_{18}-Mt	1185	0.61
Si,Fe_{30}-Mt	1180	1.08
Al,Fe_x-Mt	1180	1.12

GCMS Chromatogram

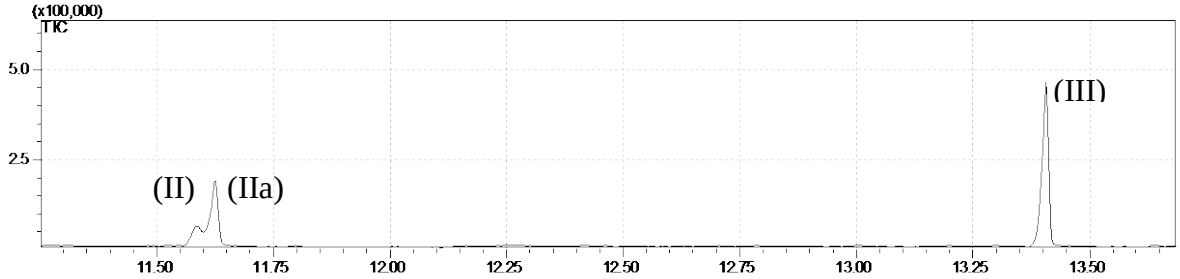

Product (II)

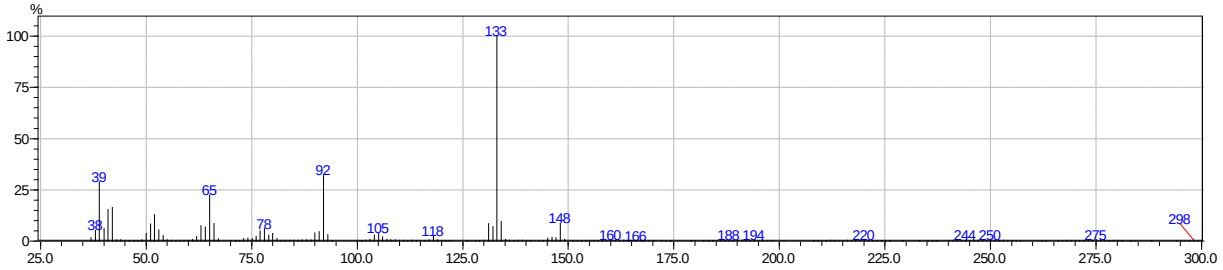

Product (IIa)

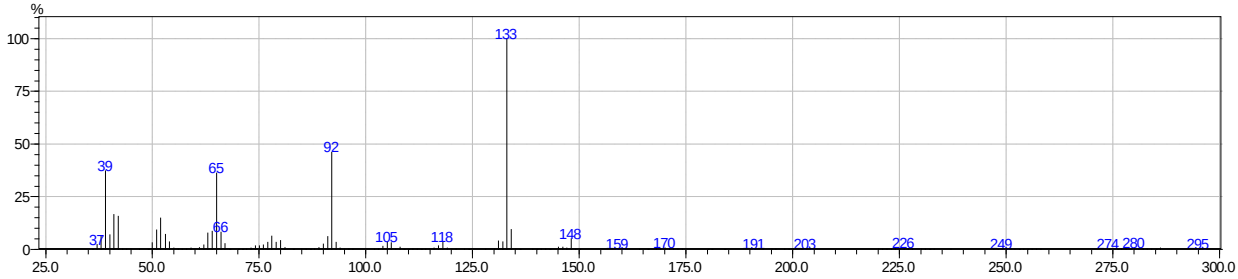

1,5-Diazepine

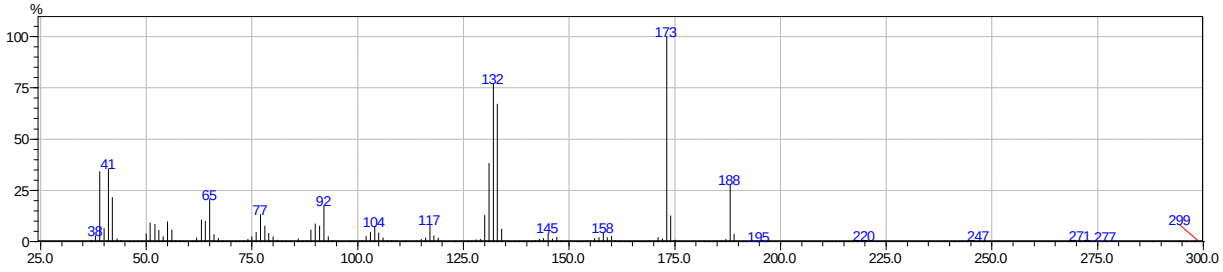

Library MS spectra of Diazepine

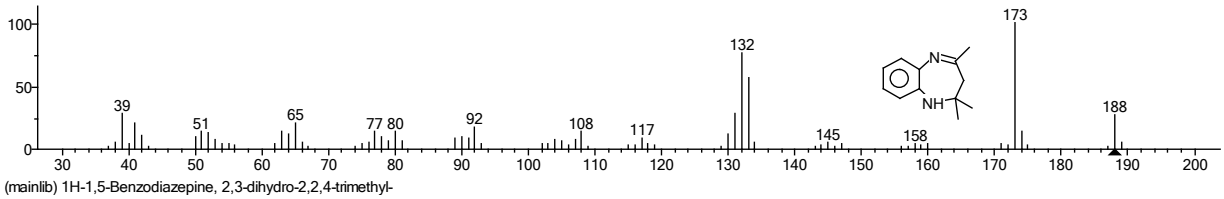

Figure S1. GCMS analysis of the reaction mixture in the presence of Al_{12},Fe_1-Mt(500).

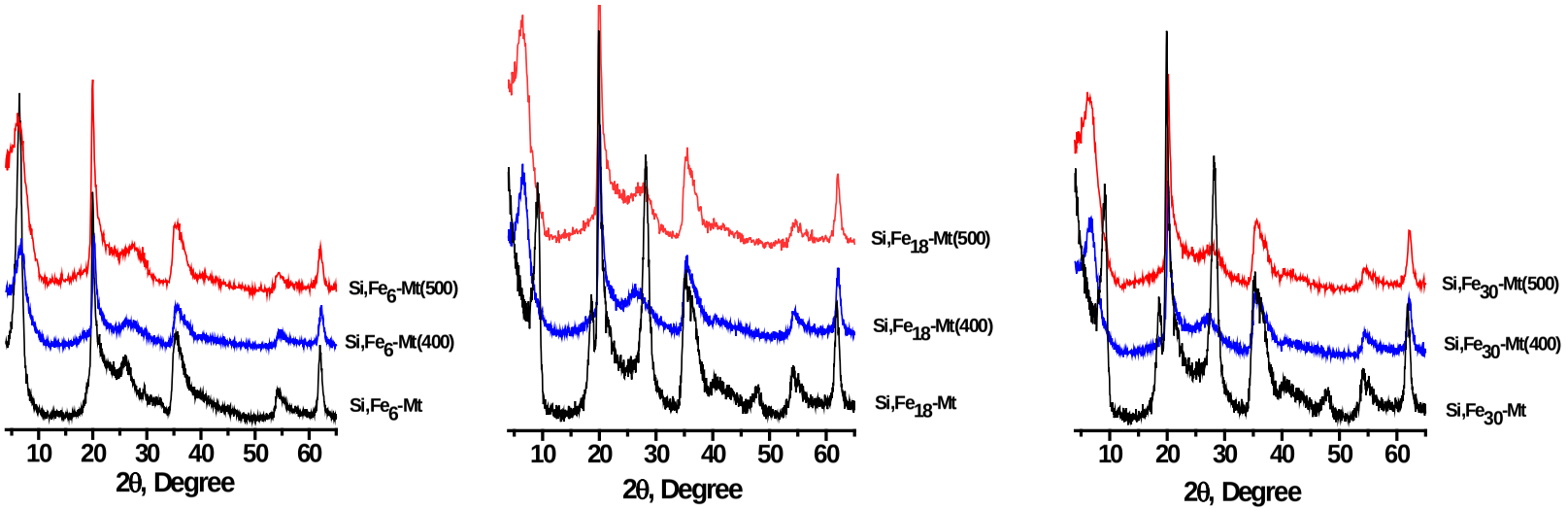

Figure S2. XRD patterns of Si,Fe_x-Mt materials.

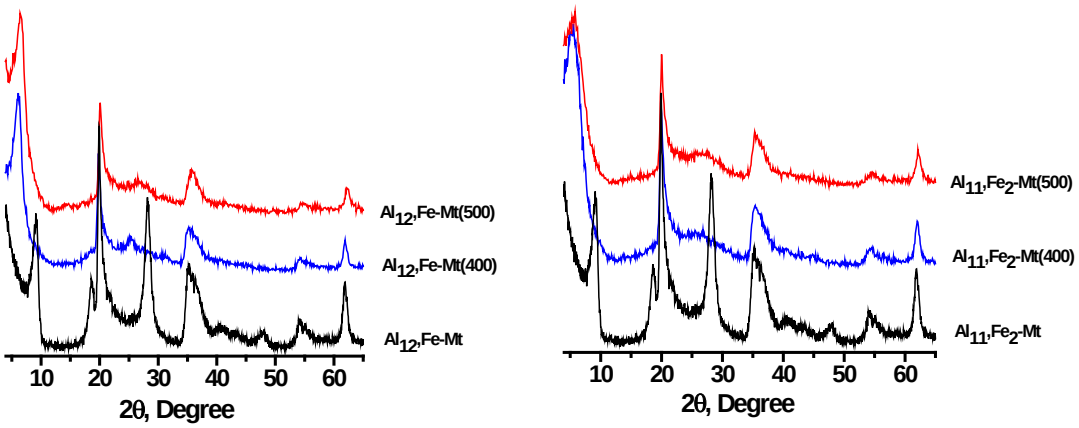

Figure S3. XRD patterns of Al,Fe_x-Mt materials.

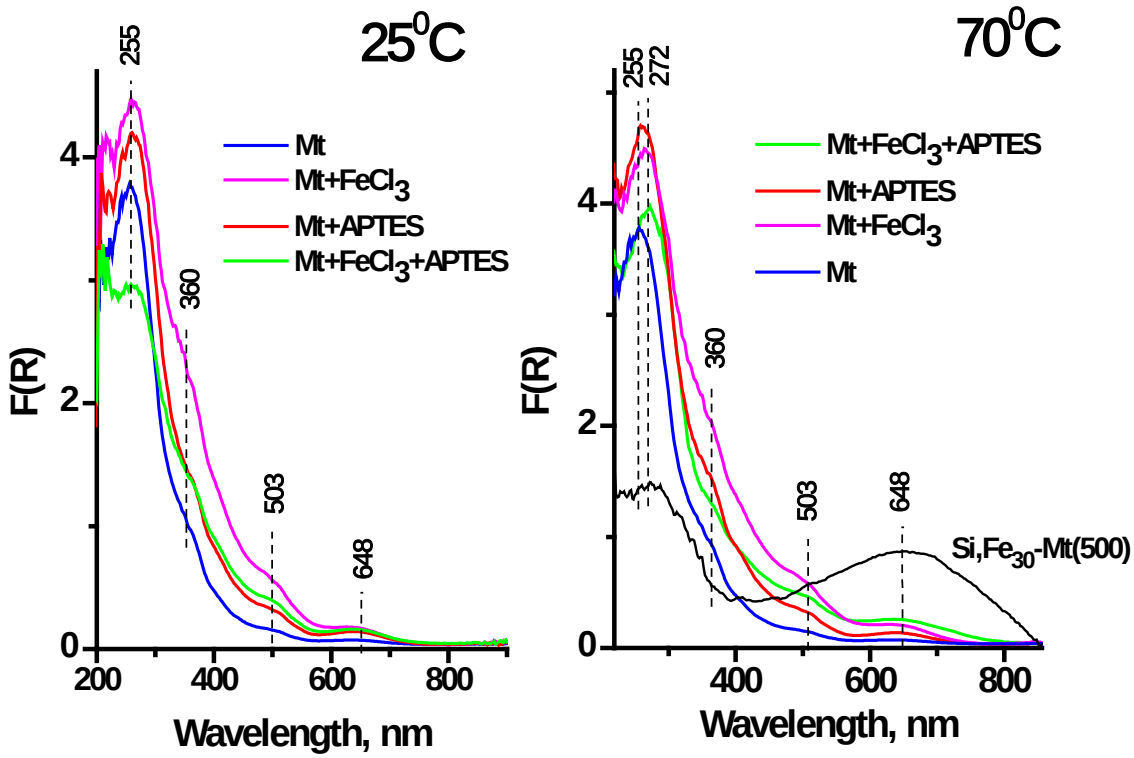

Figure S4. DR-UV-vis spectra of Mt modified by $FeCl_3$, APTES and mixture $FeCl_3$ + APTES at 25 and 70°C for 24 h.

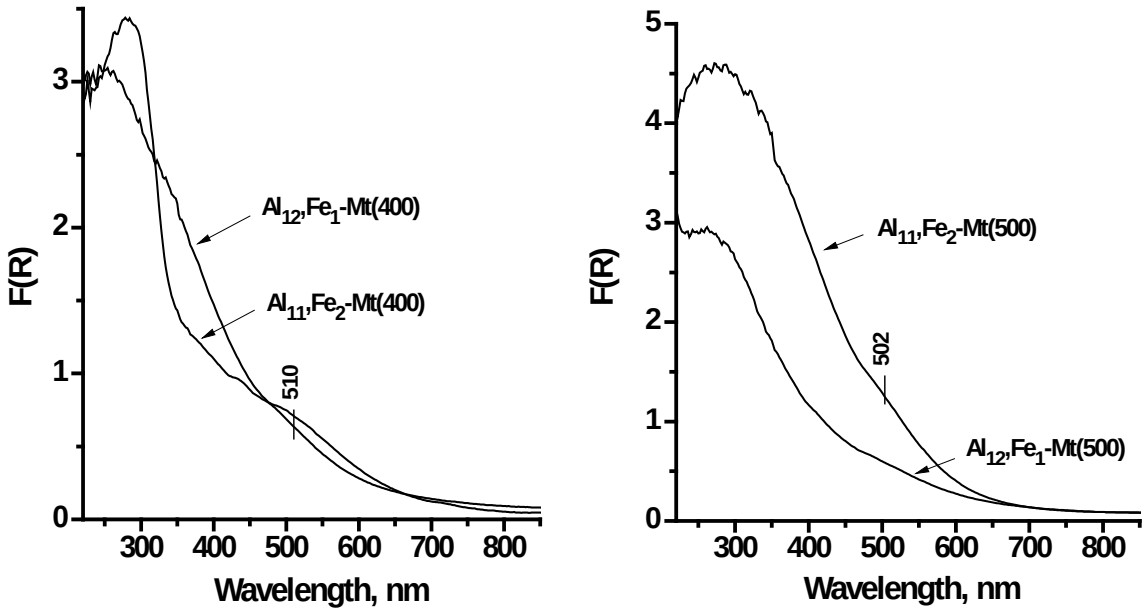

Figure S5. DR-UV-vis spectra of Al,Fe_x-Mt materials.

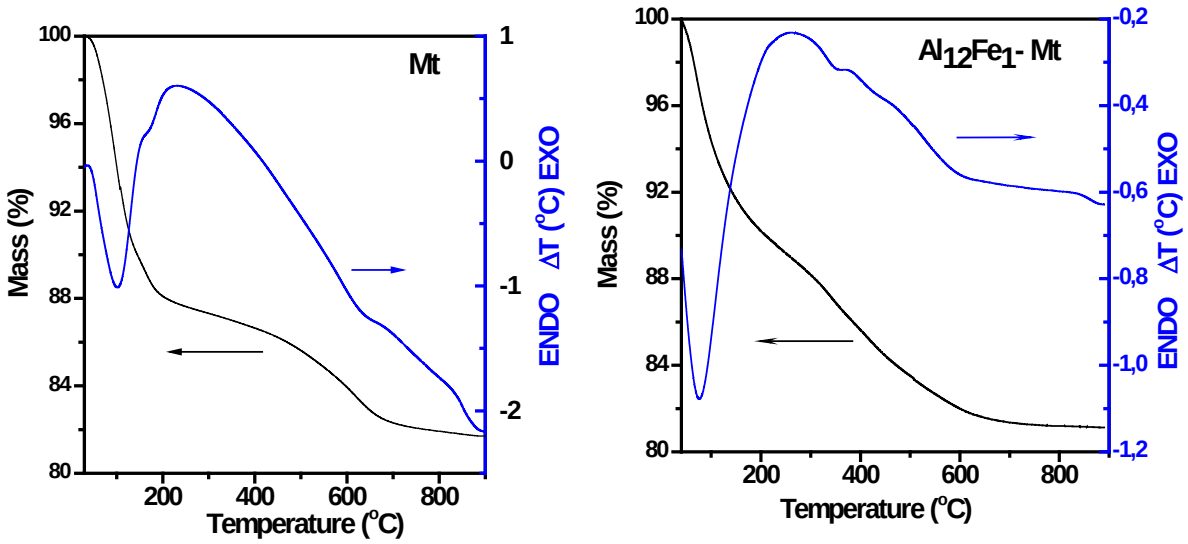

Figure S6. Thermal curves (TG and DTA) of Mt and $Al_{12}Fe_1$-Mt solids.

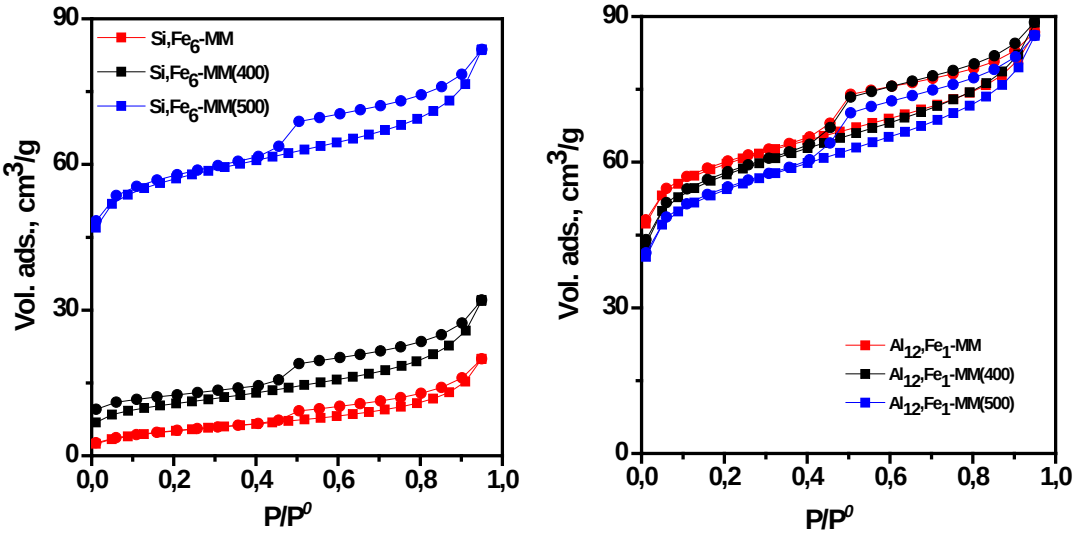

Figure S7. Nitrogen adsorption–desorption isotherms of Si,Fe_x-Mt and Al,Fe_x-Mt materials.

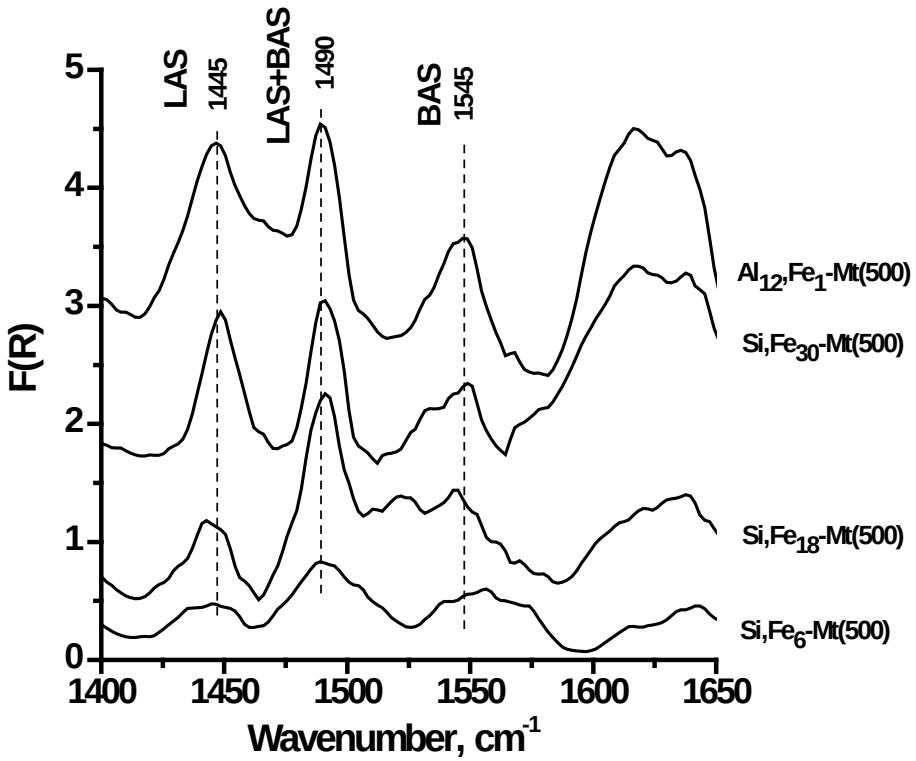

Figure S8. Difference DRIFT spectra of pyridine adsorbed on Si,Fe_x-Mt and Al,Fe_x-Mt materials.

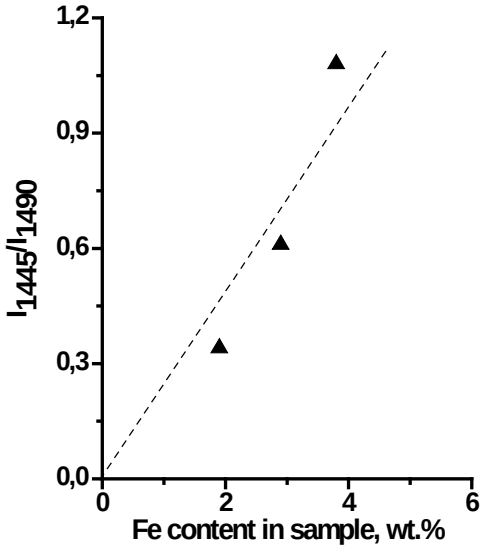

Figure S9. Correlation between I_{1445}/I_{1490} (LAS/(LAS+BAS)) ratio and Fe content in Si,Fe_x-Mt and Al_{12},Fe_1-Mt materials calcined at 500ºC (▲ - Si,Fe_x-Mt materials; ● - Al_{12},Fe_1-Mt materials).

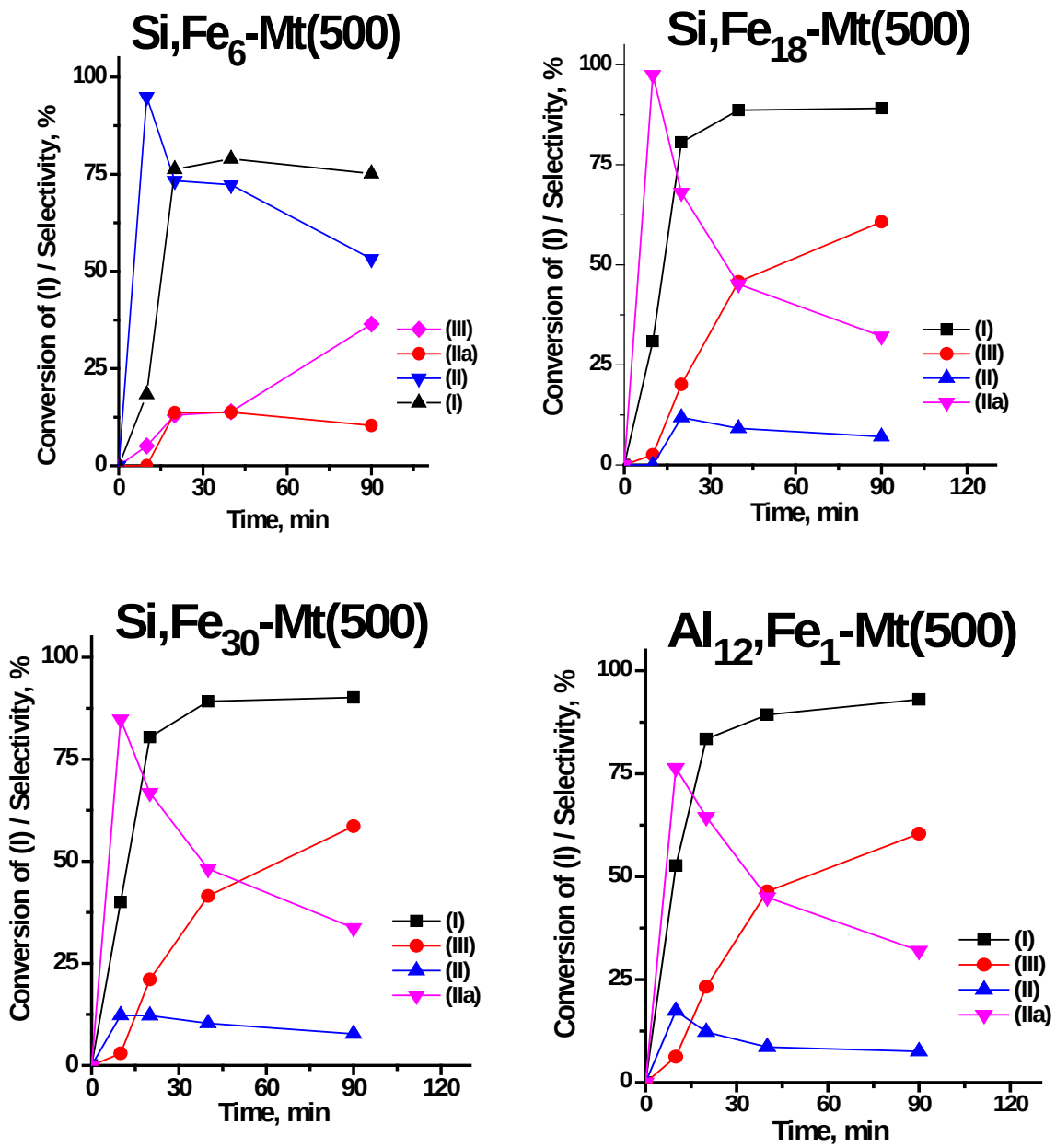

Figure S10. Kinetic curves of the cyclocondensation of (I) with acetone in the presence of Fe-containing systems calcined at 500ºC. (Reaction conditions: 0.1 mmol of (I), 0.25 mmol of acetone, 0.015 g of catalyst, 4 cm^3 of solvent, 50ºC).